Sensitivity on materials optical properties of single beam torsional Casimir actuation

Tajik, Fatemeh; Sedighi Ghozotkhar, Mehdi; Palasantzas, Georgios

Published in:
Journal of Applied Physics

DOI:
10.1063/1.4982762

Sensitivity on materials optical properties of single beam torsional Casimir actuation

Fatemeh Tajik, Mehdi Sedighi, and George Palasantzas

Citation: Journal of Applied Physics **121**, 174302 (2017); doi: 10.1063/1.4982762
View online: http://dx.doi.org/10.1063/1.4982762
View Table of Contents: http://aip.scitation.org/toc/jap/121/17
Published by the American Institute of Physics

Sensitivity on materials optical properties of single beam torsional Casimir actuation

Fatemeh Tajik,[1,2] Mehdi Sedighi,[2] and George Palasantzas[2,a)]
[1]*Department of Physics, Alzahra University, Tehran 1993891167, Iran*
[2]*Zernike Institute for Advanced Materials, University of Groningen, Nijenborgh 4, 9747 AG Groningen, The Netherlands*

(Received 8 March 2017; accepted 18 April 2017; published online 3 May 2017)

Here, we investigate the dynamical sensitivity of electrostatic torsional type microelectromechanical systems (MEMS) on the optical properties of interacting materials. This is accomplished by considering the combined effect of mechanical Casimir and electrostatic torques to drive the device actuation. The bifurcation curves and the phase portraits of the actuation dynamics have been analyzed to compare the sensitivity of a single beam torsional device operating between materials with conductivities that differ by several orders of magnitude. It is shown that the range of stable operation of torsional MEMS against stiction instabilities can increase by decreasing the conductivity of interacting materials. Moreover, the introduction of controlled dissipation, corresponding to a finite quality factor, in an otherwise unstable torsional system, could alter an unstable motion towards stiction to dissipative stable motion. *Published by AIP Publishing.*
[http://dx.doi.org/10.1063/1.4982762]

I. INTRODUCTION

Nowadays, the improvement of micro/nanofabrication technologies has given a strong impetus to device architectures deep into submicron length scales, where Casimir forces between components inevitably will play a significant role on their actuation dynamics.[1–4] These interactions between two objects arise due to fluctuations of the Electromagnetic (EM) field,[4,5] as it was predicted by Casimir in 1948[6] assuming two perfectly conducting parallel plates. A few years later, Lifshitz and co-workers in the 50s[7] considered the general case of real dielectric plates by exploiting the fluctuation-dissipation theorem, which relates the dissipative properties of matter (via optical absorption by many microscopic dipoles) and the resulting EM fluctuations. This theory describes the attractive interaction due to fluctuations of the EM field for all separations covering both the Casimir (long-range) and van der Waals (short-range) regimes.[1,7,8] In any case, the dependence of the Casimir force on materials is an important topic since in principle one can tailor the force by suitable choice of materials.[9–16]

Casimir forces could have a strong technological potential for micro/nanoelectromechanical systems (MEMS/NEMS) such as switches, accelerometers, and quantum levitation systems because they have surface areas large enough but gaps small enough for the force to draw components together, and affect their actuation dynamics.[1–4] On the other hand, the strong dependence of the Casimir force on the material optical properties[9–16] can be utilized to tune the actuation of devices. Although metals give strong Casimir forces due to the high absorption of conduction electrons in the infrared range, other materials with less conductivity but suitable for operation in harsh environments can also be used in actuating components.[17] Therefore, a suitable choice of materials could open a multitude of opportunities for device engineering and increase operation yield of these devices.

Furthermore, the broken symmetry in periodic MEMS has also attracted strong interest for contactless motion transmission. Indeed, when the translation symmetry is broken along two parallel periodic plates, it leads to creation of lateral Casimir forces.[4,19,20] Moreover, a Casimir torque can arise in systems with broken rotational symmetry.[21–23] The Casimir torque has also been investigated in optically anisotropic materials, where the torque originates from anisotropy or misalignment between the optical axes of interacting plates.[24–27] Nonetheless, the Casimir torque due to the broken rotational symmetry is stronger than that in the anisotropic systems.[22] In addition, a mechanical torque can arise in torsional electrostatic actuators due to the normal Casimir force.[28–32] The torsional actuator is constructed from two electrodes, one of which is fixed and the other is able to rotate around an axis. By applying a voltage between two electrodes, the moving electrode can rotate because of the electrostatic force, while at a certain voltage the rotating electrode can become unstable and collapse on the fixed one.[33] This dynamical behavior has been studied extensively in parallel-plate and sphere-plate geometries[17,18,34–38] by considering the interaction between materials with measured optical properties.

On the other hand, the dynamics of torsional electrostatic actuator was studied by considering the effect of van der Waals forces without including measured optical properties.[31,39] So far, however, the effect of the influence of the Casimir force on the dynamical behavior of torsional actuators made of materials with different optical properties still remains unexplored. In addition, torsional oscillators have been used for the measurement of the Casimir force,[8,28,40] underlying the importance of this type of MEMS in table top

a)Author to whom correspondence should be addressed. Electronic mail: g.palasantzas@rug.nl

cosmology to probe fundamental physics. Therefore, a realistic analysis of torsional dynamics will be performed here, where the mechanical torque due to the Casimir forces will be considered, using the measured optical properties of materials with diverse conductivities over several orders of magnitude, as input to the Lifshitz theory.

II. INFLUENCE OF OPTICAL PROPERTIES ON CASIMIR FORCES

Prior to modeling the torsional system and its actuation dynamics, we will present briefly the Lifshitz theory, which will be necessary for the calculation of the torsional Casimir torques, and illustrate the influence of different material optical properties that will be used in this study. Indeed, we consider here Au,[15] which is a good metal conductor and has been used in torsional devices,[8,40] and nitrogen doped SiC, which is a poor conductor but suitable for operation in harsh environments and well integrated in Si-based MEMS technologies.[17,36] The imaginary parts $\varepsilon''(\omega)$ of the measured frequency dependent dielectric response function $\varepsilon(\omega)$ of Au and SiC, and the corresponding functions at imaginary frequencies $\varepsilon(i\xi)$ are shown in Fig. 1. Extrapolation at low frequencies for $\varepsilon''(\omega)$, where measurements are not available, was performed using the dissipative Drude model (for details about extrapolations for low and high frequencies, see the Appendix). Differences can occur if one uses the non-dissipative plasma model[8,40] having influence also on the jump-to-contact for MEMS (details will be given elsewhere for torsional systems).[37] In any case, the ratio ω_p^2/ω_τ as obtained from the analysis of the optical data shown in Fig. 1,[15,17] where ω_p is the plasma frequency and ω_τ the damping factor in terms of the Drude model (see Appendix), yields the sample conductivity $= (\omega_p^2/\omega_\tau)/4\pi$. For SiC, we have obtained $\omega_p^2/\omega_\tau|_{SiC} = 0.4$ eV,[17] and for Au $\omega_p^2/\omega_\tau|_{Au} \approx 1600$ eV.[15] These values indicate a conductivity contrast for Au/SiC more than three orders of magnitude. Moreover, significant differences in $\varepsilon(i\xi)$ for Au and SiC appear for frequencies $\xi < 1$ eV, which will manifest to differences in the Casimir force for separations $c/2\xi > 10$ nm.

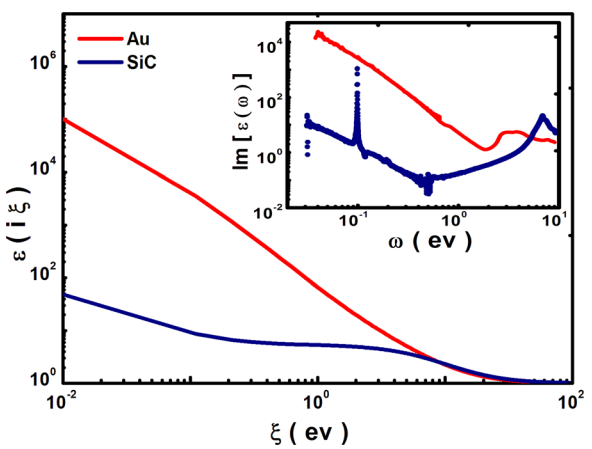

FIG. 1. Dielectric functions $\varepsilon(i\xi)$ are calculated using the Drude model for Au and conductive SiC. Here, we use the data for Au from the sample 3 in Ref. 15. The inset shows the imaginary part $\varepsilon''(\omega)$ of the frequency-dependent dielectric function measured with ellipsometry.

The non-measurable dielectric function $\varepsilon(i\xi)$ is the necessary input for the calculation of the Casimir force via the Lifshitz theory between two parallel plates at separation d and finite temperature T[7]

$$F_{Cas}(d) = \frac{k_B T}{\pi} \sum_{l=0}^{'} \sum_{\nu=TE,TM} \int_0^\infty dk_\perp k_\perp k_0 \times \frac{r_\nu^{(1)} r_\nu^{(2)} \exp(-2k_0 d)}{1 - r_\nu^{(1)} r_\nu^{(2)} \exp(-2k_0 d)}. \quad (1)$$

The prime in the first summation indicates that the term corresponding to $l = 0$ should be multiplied with a factor $1/2$. The Fresnel reflection coefficients are given by $r_{TE}^{(i)} = (k_0 - k_i)/(k_0 + k_i)$ and $r_{TM}^{(i)} = (\varepsilon_i k_0 - \varepsilon_0 k_i)/(\varepsilon_i k_0 + \varepsilon_0 k_i)$ for the transverse electric and magnetic polarizations, respectively (with ε_i the corresponding dielectric functions at imaginary frequencies). $k_{i(=0,1,2)} = (\varepsilon_i(i\xi_l) + k_\perp^2)^{1/2}$ represents the out-of plane wave vector in the gap between the plates (k_0), and in each of the interacting plates ($k_{i=(1,2)}$), as well as $k_\perp$ is the in-plane wave vector.

III. ACTUATION DYNAMICS THEORY FOR SINGLE BEAM TORSIONAL MEM

Here, we consider the electrostatic torsional actuator shown in Fig. 2, where only the upper plate can rotate without any buckling due to the applied torques. This is a cantilever type motion that applies in the limit where the cantilever does not elastically deform because we assume large beam lengths (L_x) and small torsional angles at maximum separation ($d/L_x \ll 1$). It is assumed that both plates are coated with an optically bulk coating of Au or SiC (thicknesses > 100 nm).[15,17] The initial distance when the plates are parallel is assumed to be $d = 200$ nm, and the system temperature $T = 300$ K. When a voltage V is applied between the two electrodes, the electrostatic torque will rotate the moving plate. If we denote with θ the torsional angle, the electrostatic torque is given by[32,39]

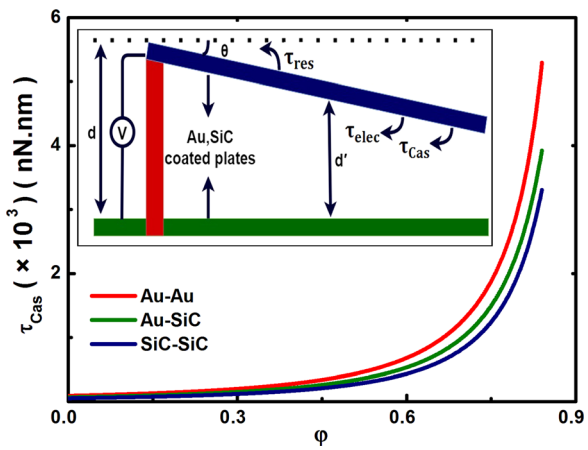

FIG. 2. Casimir torques calculated for different pairs of materials (Au-Au, Au-SiC, SiC-SiC) using as input the optical data from Fig. 1 (see also the Appendix). $\varphi = \theta/\theta_0$ is the normalized torsional angle with $\theta_0 = d/L_x$. The inset shows the schematics of the torsional MEM system at initial separation $d = 200$ nm with the acting torques indicated.

$$\tau_{elec} = \frac{1}{2}\varepsilon_0 L_y v^2 \frac{1}{\sin^2(\theta)}\left[\ln\left(\frac{d - L_x\sin(\theta)}{d}\right) + \frac{L_x\sin(\theta)}{d - L_x\sin(\theta)}\right], \tag{2}$$

where L_x and L_y are length and width of each plate, respectively (here, we consider $L_x = L_y = 10\,\mu m$), and ε_0 is the permittivity of vacuum. Any rotation of the beam will generate a torsional restoring torque

$$\tau_{res} = k\theta, \tag{3}$$

with k the torsional spring constant around the support point allowing rotation of the beam.[8,28,40,41]

Besides the electrostatic and restoring torques, a mechanical Casimir torque will also act on the rotating beam, pulling it towards the fixed plate. If we apply the proximity force approximation (PFA), where one takes the summation from all area strips $L_y dr$ contributing a torque $rF_{Cas}(d')L_y\,dr$ (with $d' = d - r\sin\theta$),[32,42] the Casimir torque is given by[31,39]

$$\tau_{Cas} = \int_0^{L_x} rF_{Cas}(d')L_y\,dr\,. \tag{4}$$

Here, we consider for simplicity flat plates because at short separations (<100 nm), nanoscale roughness can also have significant influence.[34,38,43] Since $d' = d - r\sin\theta$, one can simplify the calculations of the torque in Eq. (4) by expanding $F_{Cas}(d')$ for small θ since $\theta \ll 1$. The latter condition is satisfied since $\theta \le \theta_0\,(= d/L_x) = 0.02$. Calculations of Casimir torques for Au and SiC coated plates are shown in Fig. 2, where the mechanical torque is stronger for the Au-Au system due to higher absorption of conduction electron in the infrared range (considering the Drude model to extrapolate at low frequencies where the optical measurements are not available, see the Appendix).

If we now consider all acting torques on the moving plate, then the equation of motion for torsional system reads of the form

$$I_0\frac{d^2\theta}{dt^2} + I_0\frac{\omega}{Q}\frac{d\theta}{dt} = -\tau_{res} + \tau_{elec} + \tau_{Cas}, \tag{5}$$

where I_0 is the moment of inertia. The second term at the right hand of Eq. (5) is the intrinsic energy dissipation of the moving plate with Q the quality factor of the MEM system. In the following, we will consider high quality factors (unless it is stated otherwise) $Q \ge 10^4$,[44] so that we can neglect the effect of this term. The frequency ω is assumed to be typical for many resonators like AFM cantilever, and MEMS.[8,28,40,44]

IV. RESULTS AND DISCUSSION

Our goal is to find out under what conditions there is a periodic solution for the torsional system, which will indicate that the restoring torque is strong enough to prevent collapsing of the rotating plate onto the fixed plate. For this purpose, we introduce the bifurcation parameter $\delta_{Cas} = \tau^m_{Cas}/k\theta_0$ that represents the ratio of the minimal Casimir torque $\tau^m_{Cas} = \tau_{Cas}(\theta = 0)$, and the maximum restoring torque $k\theta_0$. A small change in δ_{Cas} can lead to an abrupt change in the actuation of the MEM system.[18,45] Using δ_{Cas}, Eq. (5) obtains the more convenient form

$$I\frac{d^2\varphi}{dt^2} = -\varphi + \delta_v\frac{1}{\varphi^2}\left[\ln(1-\varphi) + \frac{\varphi}{1-\varphi}\right] + \delta_{Cas}\left[\frac{\tau_{cas}}{\tau^m_{Cas}}\right], \tag{6}$$

with $\varphi = \theta/\theta_0$, $I = I_0/k$, and $\delta_v = (\varepsilon_0 V^2 L_y L_x^3)/(2kd^3)$ the bifurcation parameter for the electrostatic force.[30,35] The equilibrium points of Eq. (6) correspond to $\tau_{total}(= -\tau_{res} + \tau_{elec} + \tau_{Cas}) = 0$ and $d\tau_{total}/d\varphi = 0$. As a result, we obtain from Eq. (6)

$$-\varphi + \delta_v\frac{1}{\varphi^2}\left[\ln(1-\varphi) + \frac{\varphi}{1-\varphi}\right] + \delta_{Cas}\left[\frac{\tau_{cas}}{\tau^m_{Cas}}\right] = 0. \tag{7}$$

A. Strongest Casimir torque system: Au-Au

Figure 3(a) shows a plot of δ_{Cas} vs. φ for the case of Au-Au system that has the strongest Casimir torque, and different applied voltages V or equivalently different bifurcation parameters δ_v. The maximum of δ_{Cas} decreases with increasing δ_v. For a specific voltage, if the restoring torque is strong enough so that $\delta_{Cas} < \delta^{MAX}_{Cas}$, then there are two equilibrium points. The stationary points near to $\varphi = 0$ are stable centers for which periodic solutions exist around them, while the other ones close to $\varphi = 1$ are unstable saddle points. In the latter case, the torsional system is unstable during oscillation around these points due to the stronger Casimir torque leading to the collapse of the moving plate on the fixed plate, a situation known as stiction.

This can also be demonstrated by plotting δ_v versus φ, as it is shown in Fig. 3(b) for different values of δ_{Cas}. The lowest diagram in this figure is for the case of the maximum $\delta_{Cas} = 0.14$ (for V = 0 in Fig. 3(a)), and it implies that if $\delta_{Cas} > 0.14$, the torsional system will lose its stability even in the absence of any applied voltage due the strong Casimir torque. And also for $0 < \delta_{Cas} < 0.14$ and $\delta_v > 0$, there are two equilibrium points in Fig. 3(b) as it was discussed for Fig. 3(a). The critical saddle points, where the motion becomes unstable, satisfy the additional condition $d\tau_{total}/d\varphi = 0$. The latter yields from Eq. (5) the second condition for δ_{Cas} and δ_v

$$-1 + \delta_v\left[\frac{2\varphi - 3}{\varphi^2(1-\varphi)^2} + \frac{2\ln(1-\varphi)}{\varphi^3}\right] + \delta_{Cas}\frac{1}{\tau^m_{Cas}}\left(\frac{d\tau_{Cas}}{d\varphi}\right) = 0. \tag{8}$$

Besides the bifurcation analysis, the dynamics of the torsional system can be illustrated with the aid of the phase portraits that show the angular velocity $d\varphi/dt$ vs. the rotation angle φ.[46] Indeed, in Fig. 3(c) we show the phase portraits around the stable and saddle points for the case $\delta_v = 0$ (V = 0) of Fig. 3(b). Any solution with initial conditions within the homoclinic orbit that goes through the unstable saddle point (squares in Fig. 3(c)) will lead to stable motion,

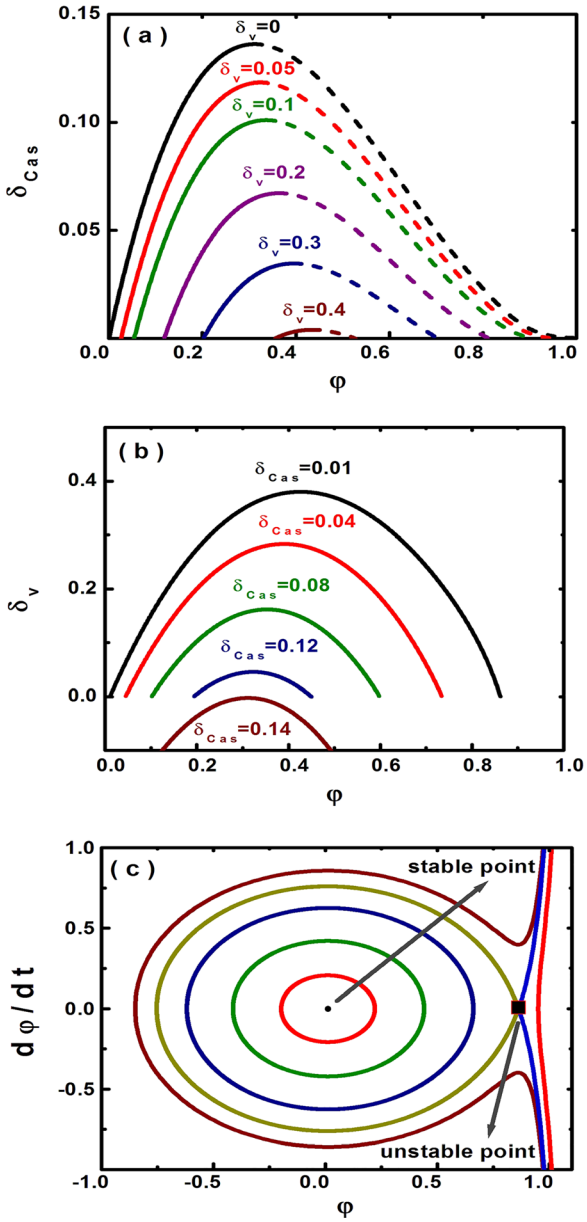

FIG. 3. (a) Bifurcation diagrams δ_{Cas} vs. φ for different δ_v for the Au-Au system. All points of the solid and dashed lines represent the stable and unstable saddle points, respectively. (b) Variation of δ_{v} for different values of δ_{Cas} for the Au-Au system. (c) Phase portraits for $\delta_{\mathrm{v}} = 0$, $\delta_{\mathrm{Cas}} = 0.01$ and initial conditions inside and outside the homoclinic orbit. The stable and unstable orbits are indicated.

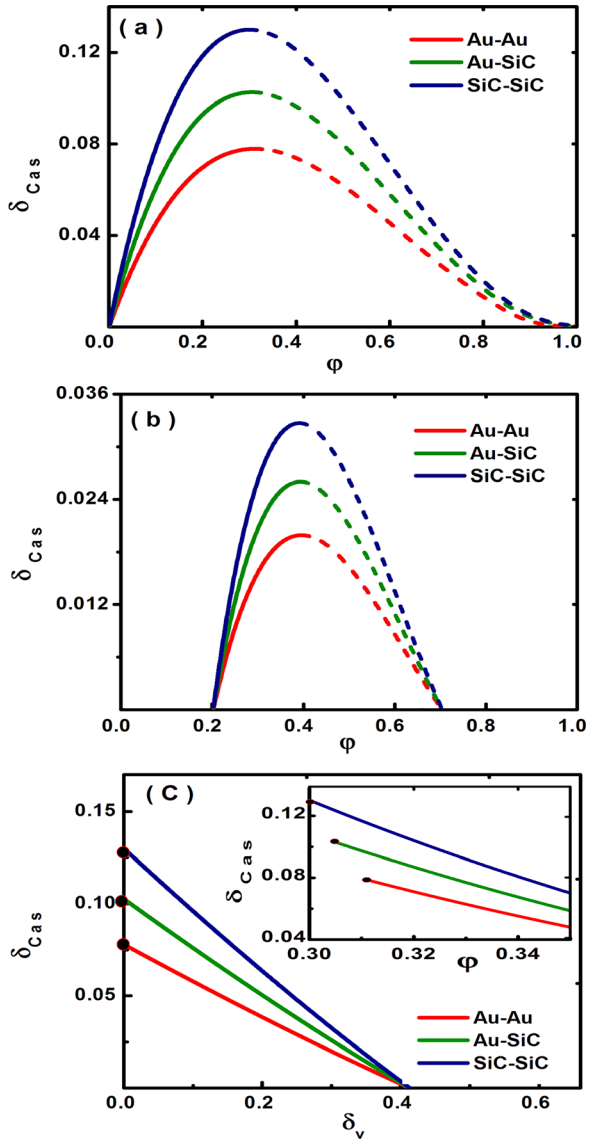

FIG. 4. Bifurcation diagrams δ_{Cas} vs. φ for material combinations Au and SiC. The solid and dashed lines represent the center and unstable saddle points, respectively. (a) $\delta_{\mathrm{v}} = 0$, and (b) $\delta_{\mathrm{v}} = 0.3$. (c) δ_{Cas} vs. δ_{v} for all combinations of Au and SiC. The inset shows δ_{Cas} vs. φ.

while for any other initial conditions outside the homoclinic orbit the upper plate will perform unstable motion leading to the collapse on the fixed plate. The periodic solutions indicate that the restoring torque is strong enough to keep system in operation and avoid any stiction instabilities.

B. Optically different material systems: Au/SiC-SiC

Having illustrated the dynamical analysis for the Au-Au, we will proceed further with the comparison between different materials. For this purpose, we considered for the minimum Casimir torque τ^m_{Cas} in Eqs. (7) and (8) its lowest value that occurs for the SiC-SiC system. Figures 4(a) and 4(b) show the bifurcation parameter δ_{Cas} is strongly sensitive to changes of the material optical properties with or without applied voltage. The region which corresponds to the stable actuation is strongly increased for the systems involving the less conductive material SiC. There are regions where the Au–Au system is unstable, while there are equilibrium points for the Au-SiC and SiC–SiC systems. Figure 4(c) shows that δ_{Cas} decreases with increasing δ_{v}, while it increases as overall with decreasing conductivity of the interacting materials. Similarly, the inset in Fig. 4(c) shows that the corresponding angle for the maximum of δ_{Cas} (circles) moves towards smaller values with decreasing conductivity. Therefore, we can infer that a torsional system, where the interacting surfaces under motion are coated with high conduction materials, will lose sooner its stability with decreasing restoring torque (since $\delta_{\mathrm{Cas}} \sim 1/\mathrm{k}$) in comparison to a system made from lower conductivity materials.

The phase portraits for different materials are presented in Figs. 5(a) and 5(b). The closed orbits, which correspond to

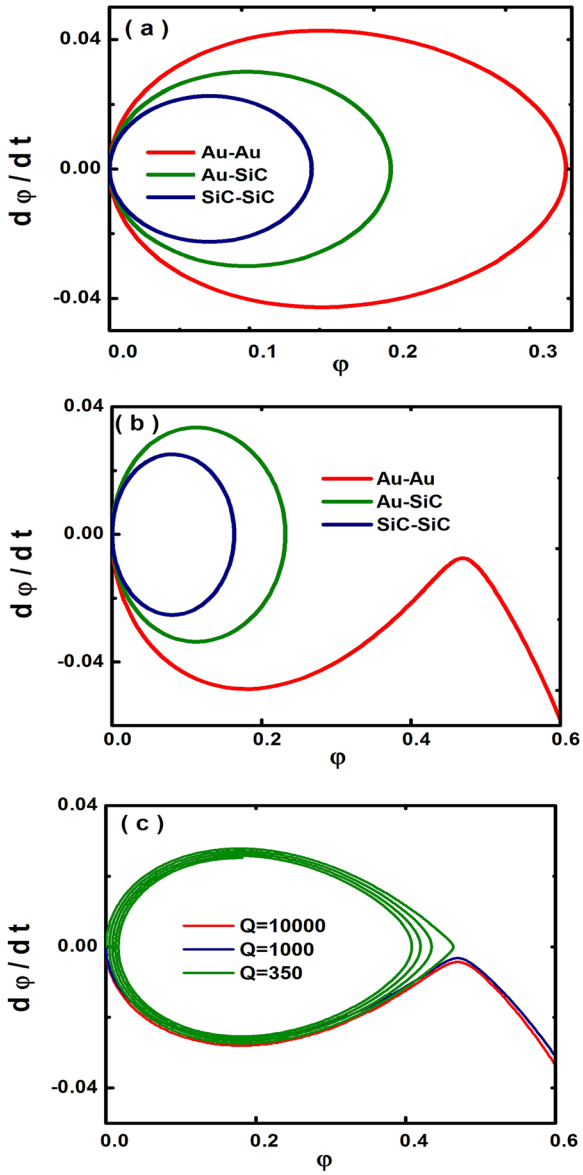

FIG. 5. (a) Phase portraits for torsional system which made from Au, SiC by using the Drude model with $\delta_{Cas} = 0.06$ and $\delta_v = 0$. (b) $\delta_{Cas} = 0.066$, $\delta_v = 0$. Closed orbits indicate stable motion, while an open orbit is the sign of unstable motion leading to stiction c. (c) Influence of the damping term on actuation dynamics of Au torsional MEMS with $\delta_{Cas} = 0.066$, $\delta_v = 0$ and different values of the quality factor Q.

periodic motion around the stable center equilibrium point, are very sensitive to changes in the material conductivity with the Au-Au system having the largest orbit due to the stronger Casimir torque, bringing the moving plate closest to the fixed plate. This is manifested in Fig. 5(b), which shows the Au-Au system to be driven rapidly to stiction, while the other systems remain functional. If, however, we increase the dissipation or equivalently reduce the quality factor Q, then it is still feasible to reduce the possibility to drive the system into stiction. For finite Q factor, Eq. (5) obtains the form

$$I\frac{d^2\varphi}{dt^2}+I\frac{\omega}{Q}\frac{d\varphi}{dt}=-\varphi+\delta_v\frac{1}{\varphi^2}\left[\ln(1-\varphi)+\frac{\varphi}{1-\varphi}\right]+\delta_{Cas}\left[\frac{\tau_{cas}}{\tau^m_{Cas}}\right]. \quad (9)$$

The effect of finite Q due to intrinsic and extrinsic dissipation mechanisms[44] of the oscillating plate is shown in Fig. 5(c). The values of the Q factor considered here are typical for a multitude of MEMS/NEMS operating in air or vacuum.[8,28,40,44] Indeed, calculations indicate that the transition from stable, but dissipative motion, to unstable motion towards stiction takes place in Fig. 5(c) for the critical quality factor $Q_C \approx 370$. The latter is typical for operation under ambient conditions.[44] Therefore, proper tuning of the system Q factor can also help to prevent the stiction of an otherwise unstable system. From Eq. (9), we can estimate the critical Q_C by setting in Eq. (7) $I(d^2\varphi/dt^2) \approx 0$ (around the critical point $\varphi = \varphi_C$ where the transition from stiction to dissipative stable motion occurs) and $d\varphi/dt = \omega$. Substitution in Eq. (9) yields for Q_C

$$\frac{1}{Q_c}-\varphi_C+\delta_v\frac{1}{\varphi_C^2}\left[\ln(1-\varphi_C)+\frac{\varphi_C}{1-\varphi_C}\right]+\delta_{Cas}\left[\frac{\tau_{cas}(\varphi_C)}{\tau^m_{Cas}}\right]. \quad (10)$$

For the conditions in Fig. 5(c) ($\delta_v = 0$, $\delta_{Cas} = 0.66$, and $\varphi_C = 0.47$), Eq. (9) yields for Q_c the numerical value $Q_c \approx 370$.

V. CONCLUSION

In conclusion, we have investigated how the dependence of the mechanical Casimir torque on the optical properties of interacting materials could play a role in the actuation dynamics of single beam torsional MEMS. The bifurcation curves and the phase portraits of the actuation dynamics have been analyzed to compare the sensitivity of a single beam torsional device operating between materials with conductivities that differ by several orders of magnitude. It is shown that the range of stable operation of torsional MEMS against stiction instabilities can increase by decreasing the conductivity of interacting materials. Moreover, the introduction of controlled dissipation, corresponding to a finite quality factor Q, in an otherwise unstable torsional system, could alter an unstable motion towards stiction to dissipative stable motion. Therefore, the proper choice of the conductivity of interacting materials in torsional MEM systems, and the tuning of energy dissipation, can help to maximize their regime of stable operation.

ACKNOWLEDGMENTS

G.P. would like to acknowledge support from the Zernike Institute for Advanced Materials and the FOM Grant No. 104206, and F.T. acknowledges funding from the Ministry of Science, Research and Technology, Iran and Alzahra University. We would like also to thank V. B. Svetovoy for useful discussions.

APPENDIX: ANALYSIS AND CALCULATION OF OPTICAL PROPERTIES

$\varepsilon(i\xi)$ is the dielectric function evaluated at imaginary frequencies, which is necessary for calculating the Casimir force between real materials using the Lifshitz theory. Using the Kramers-Kronig relation, $\varepsilon(i\xi)$ is given by[7]

$$\varepsilon(i\xi) = 1 + \frac{2}{\pi}\int_0^\infty \frac{\omega\,\varepsilon''(\omega)}{\omega^2 + \xi^2}\,d\omega. \tag{A1}$$

For the calculation of the integral in Eq. (A1), one needs the measured data for the imaginary part $\varepsilon''(\omega)$ of the frequency dependent dielectric function $\varepsilon(\omega)$. The latter are shown in Fig. 1 for Au and SiC. Both type of materials were optically characterized by ellipsometry over a wide range of frequencies (J. A. Woollam Co., VUV-VASE (0.5–9.34 eV) and IR-VASE (0.03–0.5 eV)).[15,17,36] The experimental data for the imaginary part of dielectric function cover only a limit range of frequencies $\omega_1 (= 0.03\,\text{ev}) < \omega < \omega_2 (= 8.9\,\text{ev})$. Therefore, for the low optical frequencies ($\omega < \omega_1$) we extrapolated using the Drude model for the imaginary part[15,17]

$$\varepsilon''_{\rm L}(\omega) = \frac{\omega_{\rm p}^2\,\omega_\tau}{\omega\left(\omega^2 + \omega_\tau^2\right)}, \tag{A2}$$

where $\omega_{\rm p}$ is the plasma frequency, and ω_τ is the relaxation frequency. And for the high optical frequencies ($\omega > \omega_2$), we extrapolated using the expression[15,17,36]

$$\varepsilon''_{\rm H}(\omega) = \frac{\rm A}{\omega^3}. \tag{A3}$$

Using Eqs. (A1)–(A3), $\varepsilon(i\xi)$ is given by[17,36]

$$\varepsilon(i\xi) = 1 + \frac{2}{\pi}\int_0^{\omega_1} \frac{\omega\,\varepsilon''_{\rm exp}(\omega)}{\omega^2 + \xi^2}\,d\omega + \Delta_{\rm L}\varepsilon(i\xi) + \Delta_{\rm H}\varepsilon(i\xi), \tag{A4}$$

with

$$\begin{aligned}\Delta_{\rm L}\varepsilon(i\xi) &= \frac{2}{\pi}\int_0^{\omega_1} \frac{\omega\,\varepsilon''_{\rm L}(\omega)}{\omega^2 + \xi^2}\,d\omega \\ &= \frac{2\omega_{\rm p}^2\omega_\tau}{\pi\left(\xi^2 - \omega_\tau^2\right)}\left[\frac{\arctan\left(\frac{\omega_1}{\omega_\tau}\right)}{\omega_\tau} - \frac{\arctan\left(\frac{\omega_1}{\xi}\right)}{\xi}\right]\end{aligned} \tag{A5}$$

and

$$\begin{aligned}\Delta_{\rm H}\varepsilon(i\xi) &= \frac{2}{\pi}\int_{\omega_2}^\infty \frac{\omega\,\varepsilon''_{\rm H}(\omega)}{\omega^2 + \xi^2}\,d\omega \\ &= \frac{2\omega_2^3\,\varepsilon''(\omega_2)}{\pi\xi^2}\left[\frac{1}{\omega_2} - \frac{\frac{\pi}{2} - \arctan\left(\frac{\omega_2}{\xi}\right)}{\xi}\right].\end{aligned} \tag{A6}$$

[1] A. W. Rodriguez, F. Capasso, and S. G. Johnson, Nat. Photonics **5**, 211 (2011).
[2] F. Capasso, J. N. Munday, D. Iannuzzi, and H. B. Chan, IEEE J. Sel. Top. Quantum Electron. **13**, 400 (2007).
[3] P. Ball, Nature **447**, 772 (2007).
[4] M. Bordag, G. L. Klimchitskaya, U. Mohideen, and V. M. Mostepanenko, *Advances in the Casimir Effect* (Oxford University Press, New York, 2009).
[5] P. W. Milonni, *The Quantum Vacuum: An Introduction to Quantum Electrodynamics* (Academic Press, 1993).
[6] H. B. G. Casimir, Proc. K. Ned. Akad. Wet. **51**, 793 (1948).
[7] E. M. Lifshitz, Sov. Phys. - JETP **2**, 73 (1956); I. E. Dzyaloshinskii, E. M. Lifshitz, and L. P. Pitaevskii, Sov. Phys. Usp. **4**, 153 (1961).
[8] R. S. Decca, D. López, E. Fischbach, G. L. Klimchitskaya, D. E. Krause, and V. M. Mostepanenko, Ann. Phys. **318**, 37 (2005); S. K. Lamoreaux, Phys. Rev. Lett. **78**, 5 (1997); Rep. Prog. Phys. **68**, 201 (2005); H. B. Chan, V. A. Aksyuk, R. N. Kleiman, D. J. Bishop, and F. Capasso, Phys. Rev. Lett. **87**, 211801 (2001); Science **291**, 1941 (2001).
[9] D. Iannuzzi, M. Lisanti, and F. Capasso, Proc. Natl. Acad. Sci. U.S.A. **101**, 4019 (2004).
[10] F. Chen, G. L. Klimchitskaya, V. M. Mostepanenko, and U. Mohideen, Opt. Express **15**, 4823 (2007); G. Torricelli, I. Pirozhenko, S. Thornton, A. Lambrecht, and C. Binns, Europhys. Lett. **93**, 51001 (2011).
[11] S. de Man, K. Heeck, R. J. Wijngaarden, and D. Iannuzzi, Phys. Rev. Lett. **103**, 040402 (2009).
[12] G. Torricelli, P. J. van Zwol, O. Shpak, C. Binns, G. Palasantzas, B. J. Kooi, V. B. Svetovoy, and M. Wuttig, Phys. Rev. A **82**, 010101 (R) (2010).
[13] G. Torricelli, P. J. van Zwol, O. Shpak, G. Palasantzas, V. B. Svetovoy, C. Binns, B. J. Kooi, P. Jost, and M. Wuttig, Adv. Funct. Mater. **22**, 3729 (2012).
[14] C.-C. Chang, A. A. Banishev, G. L. Klimchitskaya, V. M. Mostepanenko, and U. Mohideen, Phys. Rev. Lett. **107**, 090403 (2011).
[15] V. B. Svetovoy, P. J. van Zwol, G. Palasantzas, and J. Th. M. DeHosson, Phys. Rev. B. **77**, 035439 (2008); G. Bimonte, Phys. Rev. A **83**, 042109 (2011).
[16] A. Canaguier-Durand, P. A. Maia Neto, A. Lambrecht, and S. Reynaud, Phys. Rev. A **82**, 012511 (2010).
[17] M. Sedighi, V. B. Svetovoy, W. H. Broer, and G. Palasantzas, Phys. Rev. B **89**, 195440 (2014).
[18] M. Sedighi, W. H. Broer, G. Palasantzas, and B. J. Kooi, Phys. Rev. B **88**, 165423 (2013).
[19] H.-C. Chiu, G. L. Klimchitskaya, V. N. Marachevsky, V. M. Mostepanenko, and U. Mohideen, Phys. Rev. B **81**, 115417 (2010); F. Chen, U. Mohideen, G. L. Klimchitskaya, and V. M. Mostepanenko, Phys. Rev. A **66**, 032113 (2002); T. Emig, A. Hanke, R. Golestanian, and M. Kardar, *ibid.* **67**, 022114 (2003).
[20] F. Chen, U. Mohideen, G. L. Klimchitskaya, and V. M. Mostepanenko, Phys. Rev. Lett. **88**, 101801 (2002).
[21] R. B. Rodrigues, P. A. Maia Neto, A. Lambrecht, and S. Reynaud, J. Phys. A: Math. Theor. **41**, 164019 (2008).
[22] R. Guérout, A. Lambrecht, S. Reynaud, and C. Gent, Euro. Phys. Lett. **111**, 44001 (2015).
[23] R. B. Rodrigues, P. A. Maia Neto, A. Lambrecht, and S. Reynaud, Eur. Phys. Lett.**76**, 822 (2006).
[24] J. N. Munday, D. Iannuzzi, Y. Barash, and F. Capasso, Phys. Rev. A **71**, 042102 (2005).
[25] J. N. Munday, D. Iannuzzi, and F. Capasso, New J. Phys.**8**, 244 (2006).
[26] T. G. Philbin and U. Leonhardt, Phys. Rev. A **78**, 042107 (2008).
[27] X. Chen and J. C. H. Spence, Phys. Status Solidi A **210**(9), 1925 (2013).
[28] F. Intravaia, S. Koev, L. W. Jung, A. A. Talin, P. S. Davids, R. S. Decca, V. A. Aksyuk, D. A. R. Dalvit, and D. López, Nat. Commun. **4**, 2515 (2013).
[29] Y. Nemirovsky and O. Degani, J. Microelectromech. Syst. **10**, 601 (2001).
[30] O. Degani and Y. Nemirovsky, J. Microelectromech. Syst. **11**, 20 (2002).
[31] J. G. Guo and Y. P. Zhao, Int. J. Solids Struct. **43**, 675 (2006).
[32] R. Satter, F. Plötz, G. Fattinger, and G. Wachutka, Sens. Actuators, A **97–98**, 337 (2002).
[33] O. Bochobza-Degani and Y. Nemirovsky, Sens. Actuators, A **97–98**, 569 (2002).
[34] W. Broer, G. Palasantzas, J. Knoester, and V. B. Svetovoy, Phys. Rev. B **87**, 125413 (2013).
[35] G. Palasantzas and J. Th. M. De Hosson, Phys. Rev. B **72**, 115426 (2005).
[36] M. Sedighi, V. B. Svetovoy, and G. Palasantzas, Phys. Rev. B **93**, 085434 (2016).
[37] M. Sedighi, W. H. Broer, S. Van der Veeke, V. B. Svetovoy, and G. Palasantzas, J. Phys.: Condens. Matter **27**, 214014 (2015); M. Sedighi and G. Palasantzas, J. Appl. Phys. **117**, 144901 (2015).
[38] W. Broer, H. Waalkens, V. B. Svetovoy, J. Knoester, and G. Palasantzas, Phys. Rev. Appl. **4**, 054016 (2015).
[39] W. H. Lin and Y. P. Zhao, J. Phys. D: Appl. Phys. **40**, 1649 (2007).
[40] R. S. Decca, D. López, E. Fischbach, G. L. Klimchitskaya, D. E. Krause, and V. M. Mostepanenko, Phys. Rev. D **75**, 077101 (2007).

[41]O. Degani, E. Socher, A. Lipson, T. Lejtner, D. J. Setter, Sh. Kaldor, and Y. Nemirovsky, J. Microelectromech. Syst. **7**, 373 (1998).
[42]W. H. Lin and Y. P. Zhao, Chaos, Solitons Fractals **23**, 1777 (2005).
[43]V. B. Svetovoy and G. Palasantzas, Adv. Colloid Interface Sci. **216**, 1 (2015); G. Palasantzas, V. B. Svetovoy, and P. J. van Zwol, Int. J. Mod. Phys. B **24**, 6013 (2010).
[44]R. Garcıa and R. Perez, Surf. Sci. Rep. **47**, 197 (2002); M. Li, H. X. Tang, and M. L. Roukes, Nat. Nanotechnol. **2**, 114 (2007).
[45]S. Cui and Y. C. Soh, J. Microelectromech. Syst. **19**, 1153 (2010).
[46]M. W. Hirsch, S. Smale, and R. L. Devaney, *Differential Equations, Dynamical Systems, and an Introduction to Chaos* (Elsevier Academic Press, San Diego, CA, 2004).